Nuclear Inst. and Methods in Physics Research, A 904 (2018) 163–170

Contents lists available at ScienceDirect

Nuclear Inst. and Methods in Physics Research, A

journal homepage: www.elsevier.com/locate/nima

Baseline restoration method based on mathematical morphology for high-pressure xenon detectors

Le Gao [a], Xiaobin Tang [a,b,*], Pin Gong [a,b], Wen Yan [a], Maheng Ye [a], Peng Wang [c], Jinzhao Zhang [d]

[a] Department of Nuclear Science and Engineering, Nanjing University of Aeronautics and Astronautics, Nanjing 210016, China
[b] Jiangsu Key Laboratory of Nuclear Energy Equipment Materials Engineering, Nanjing University of Aeronautics and Astronautics, Nanjing 210016, China
[c] School of Environmental and Biological Engineering, Nanjing University of Science and Technology, Nanjing 210094, China
[d] National Ocean Technology Center, Tianjin 300112, China

ARTICLE INFO

Keywords:
Baseline restoration
High-pressure xenon detector
Mathematical morphology
Field programmable gate array
External acoustic noise

ABSTRACT

The shift of baseline has always existed in high-pressure xenon (HPXe) detectors because of the influence of external acoustic noise. This problem seriously influences the spectrometric characteristics of these detectors. A special baseline restoration method is required to remove the shift of baseline in real time. This study demonstrated that the top hat transform based on mathematical morphology can restrain the shift of baseline in digital multichannel analyzer. An improved baseline restoration (IBLR) method based on mathematical morphology was proposed and implemented in field programmable gate array (FPGA) to obtain superior baseline restoration. The structuring element of the IBLR method can be adjusted automatically in real time according to the characteristics of the baseline. Experimental results show that the IBLR method can maintain an excellent energy resolution over a wide shift range of baseline. To strengthen our conclusion, we carried out an external acoustic noise experiment on a HPXe detector. The HPXe detector with IBLR was virtually unaffected by external acoustic noise.

1. Introduction

With the widespread application of nuclear technology, radiation monitoring with high energy resolution detectors is required for extreme environments such as wide temperature variations or high radiation exposures [1–3]. High-pressure xenon (HPXe) detectors with excellent energy resolution [4,5] have good physical characteristics such as wide operating temperature range (from −20 °C to 100 °C) [6], high radiation resistance [7], and long term performance [8]; these characteristics are suitable for radiation detection in extreme environments [9,10]. However, these devices still have a serious shortcoming, that is high sensitivity to external acoustic noise (vibroacoustic effects) [11–13]. When a HPXe detector is affected by external acoustic noise, the detector's spectrometric characteristic deteriorates significantly. This problem makes HPXe detectors more operate in laboratory and limits its applications in some strong acoustic noise environments, such as airborne radiation monitoring, radiation customs control, and orbital station radiation monitoring.

HPXe detectors without vibroacoustic effects will have a widespread application prospect because of the high energy resolution and good physical characteristics. Thus, many methods have been used to remove the vibroacoustic effects of HPXe detectors. Different shock and sound absorbers are used to protect HPXe detectors from vibroacoustic effects, but they are not always efficient and lead to a notable increase of equipment mass and size [14]. The cylindrical ionization chamber with a Frisch grid made from electrochemically etched foil has higher stability to vibroacoustic effects over a wide range of noise levels [15]. The implementation of a digital third order Butterworth filter effectively mitigates the vibroacoustic effects [16]. Novikov et al. [17] proposed that the presence of high external acoustic perturbations alters the capacitance between the Frisch grid and the anode, resulting in a corresponding shift of baseline. In addition, the resistance to acoustic noise is achieved by removing the shift of baseline through digital signal processing. Although these methods have positive resistance effect to the vibroacoustic effects, the energy resolution still evidently deteriorates as external acoustic noise increases. Compared with other methods, the digital signal processing method has better performance in terms of resistance effect and flexibility. Thus, removing the shift of baseline by digital signal processing is an ideal way to eliminate the vibroacoustic effects of HPXe detectors.

In the current work, the feasibility of baseline restoration based on mathematical morphology was demonstrated. For superior performance under serious shift of baseline, the improved baseline restoration (IBLR) method based on mathematical morphology was proposed and implemented; this method can automatically adjust the structuring element

* Corresponding author at: Department of Nuclear Science and Engineering, Nanjing University of Aeronautics and Astronautics, Nanjing 210016, China.
E-mail address: tangxiaobin@nuaa.edu.cn (X. Tang).

https://doi.org/10.1016/j.nima.2018.07.040
Received 10 May 2018; Received in revised form 12 July 2018; Accepted 14 July 2018
Available online 17 July 2018
0168-9002/

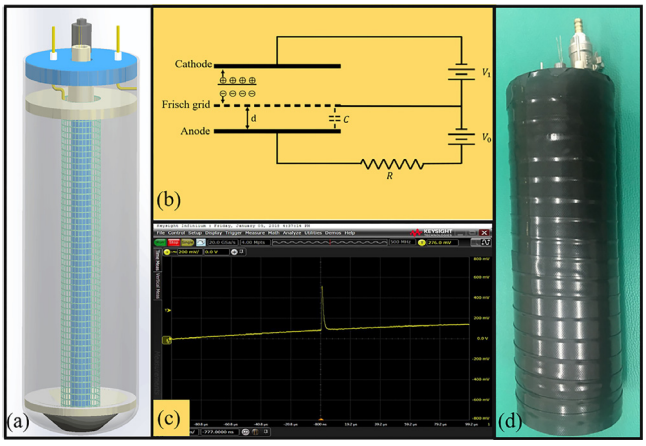

Fig. 1. HPXe detector: (a) structure of HPXe detector, (b) schematic of HPXe detector, (c) the shift of baseline in HPXe detector under external acoustic noise, (d) prototype of "Nucl-x-HPXe".

according to the characteristic of the baseline. Moreover, HPXe detectors with IBLR can operate under high external acoustic noise.

2. Method and principle

2.1. Experimental device

The HPXe detector is the pulse ionization chamber with a Frisch grid, and the dependence of the pulse amplitude on position of interaction in electron-sensitive ion chambers can be removed through the use of the structure with a Frisch grid [18] shown in Fig. 1(a). However, when the HPXe detector is exposed to external acoustic noise, the Frisch grid resonates with the acoustic noise. The detector capacitance between the Frisch grid and the anode is altered due to the vibration of the Frisch grid. Therefore, the corresponding shift of the baseline occurs in strong acoustic noise environment (Fig. 1(c)), the nuclear pulses are superimposed on the corresponding shift of the baseline. In the noise characteristics, it is the low-frequency noise which frequency is depended on the frequency of acoustic noise environment. The HPXe detector used in this work is the "Nucl-x-HPXe" designed by our laboratory (Fig. 1(d)), and it was designed by reference to Moscow Engineering Physics Institute (MEPhI) [19].

The "Nucl-x-HPXe" detector is a cylindrical pulse ionization chamber filled with Xe + 0.3% H_2 mixture. The xenon is pressurized to achieve a nominal density of 0.3 g/cm^3 at 50 atm. The gas purity can reach the value that corresponds to the electrons' lifetime of 1 ms. The detector has an outside diameter of about 106 mm and an active diameter of about 100 mm. The detector's sensitive volume is 2 liters. The anode diameter and shielding grid diameter are 20 mm and 36 mm respectively. The voltage of cathode and shielding grid are −20 kV and −12.5 kV. Therefore, The signal is measured from the anode through the charge sensitive preamplifier.

The focus of this study is the removal of the shift of baseline caused by external acoustic noise; thus, a special baseline restoration should be designed in digital multichannel analyzer (DMCA). When the detector is exposed to external acoustic noise, the baseline of detector signal will shift. We defines the difference between the highest and lowest baseline values as the shift levels of baseline. The shift level of baseline is not easy to control accurately by external acoustic noise. To evaluate the performance of baseline restorations, we added an adjustable shift of baseline to the HPXe detector's signal as test signals in a quiet environment. The adjustable shift of baseline was a 1000 Hz sinusoidal signal generated by a signal generator (RIGOL DG4062), because previous research showed that HPXe detectors reached the highest sensitivity to

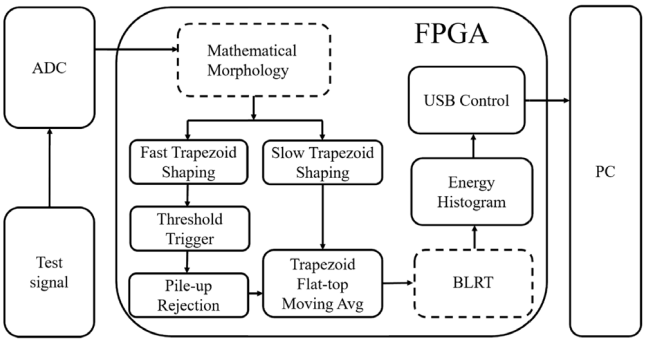

Fig. 2. Block diagram of DMCA in FPGA, mathematical morphology method: upper left dotted box; BLRT method: bottom right dotted box; NBLR: without dotted boxes.

1000 Hz sinusoidal noise [16]. Different sinusoidal signal amplitudes (0–900 mV) provided different slopes and highs of the baseline, and the 900 mV sinusoidal signal is similar to the shift level of baseline caused by 90 dB in this study. In addition, there is approximately an exponential relationship between shift level of baseline and external acoustic noise.

Baseline restorations can be implemented in DMCA, which was designed by our laboratory in field programmable gate array (FPGA). The block diagram of the DMCA in FPGA is shown in Fig. 2. Test signals were digitized by a high-speed ADC (AD9226) for digital signal processing in the FPGA (Altera EP4CE). Different baseline restoration methods such as the mathematical morphology method, baseline restoration of trapezoidal pulse shaping (BLRT) [20] and no baseline restoration (NBLR) were studied. In addition, the test signals were connected to an Ortec model 926 multichannel buffer for comparison.

2.2. Mathematical morphology

Mathematical morphology is a technique for analyzing and processing geometrical structures. Mathematical morphology filter is different from common filtering methods that transform between the time and frequency domains; it is based on integral geometry and stochastic theory and does not involve difficult mathematical transformations and formulas. The goal of mathematical morphology transformations is to maintain the morphological characteristics and eliminate noise effectively. In recent years, mathematical morphology has been used in one-dimensional signal processing, such as electrocardiogram and Raman spectrum background subtraction [21,22], because it requires minimal calculation without an iteration procedure and it shows an excellent processing effect. The goal of baseline restoration is to maintain pulse amplitude and eliminate the shift of baseline effectively; thus, it is a suitable method to solve the shift of baseline in HPXe detectors.

Most morphological operations are based on erosion and dilation, and the effect of morphological operations depend on the structuring element [23]. Fig. 3(a) shows the erosion and dilation of a ideal negative exponent signal which is generated from the MATLAB. The dilation expands the signal upward, and the pulse amplitude information is retained. The erosion shrinks the signal downward, and the bottom profile of signal is recorded. The degree of expansion and shrinkage depends on the height of the structuring element, and the length of the structuring element should be longer than the negative exponent pulse [24]. The result obtained by erosion operation continues to be operated by the dilation operation, and the result of opening operation (Erosion-Dilation) is shown in Fig. 3(b). An estimated baseline, which overlaps with the bottom of the signals can be obtained by the opening operation. Thus, the shift of baseline can be solved by subtracting the estimated baseline from the original signal; this method is called top hat transform (THT) in mathematical morphology.

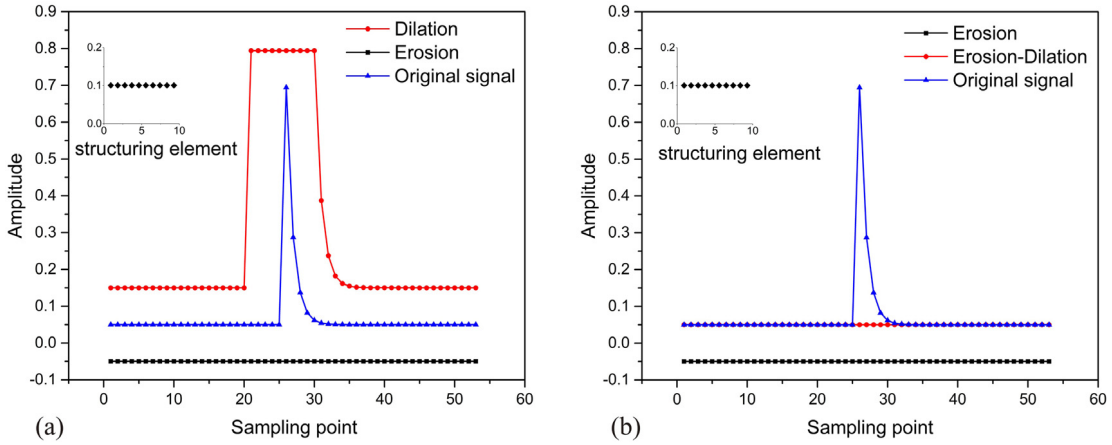

Fig. 3. Illustration of morphological operations: (a) erosion and dilation and (b) opening operation. (For interpretation of the references to colour in this figure legend, the reader is referred to the web version of this article.)

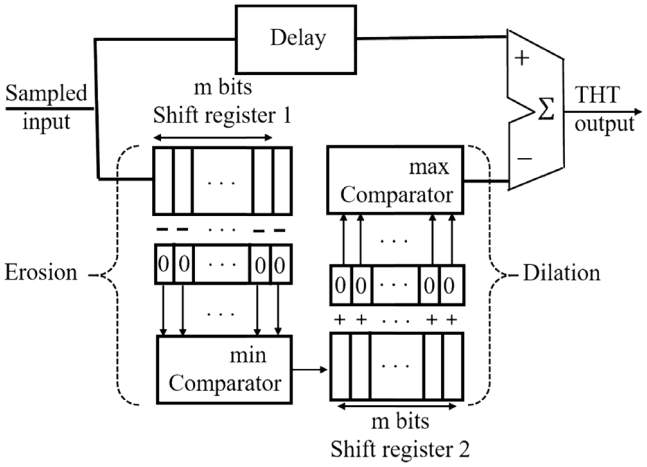

Fig. 4. Implementation of the THT method in FPGA.

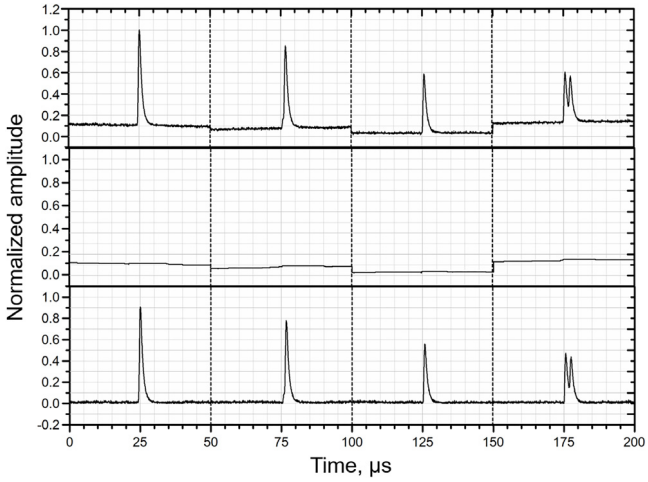

Fig. 5. Fragments of digital signals under 300 mV shift of baseline in SignalTap ii (top: test signal; middle: estimated baseline; bottom: signal after the THT method).

3. THT baseline restoration method

3.1. Design of the THT baseline restoration algorithm in FPGA

The THT method can be easily implemented in FPGA; it deals with the shift of baseline before trapezoidal pulse shaping. The logic diagram of the THT algorithm in FPGA is shown in Fig. 4. A flat structuring element (0, 0 … , 0) is selected [25], and the length of the structuring element is *m*. The shift registers aligned with the structuring element are moving windows. The structuring element is subtracted (added) from (to) the data in these moving windows, and then the minimum (maximum) value is obtained from the front calculation results by the comparators, that is, the erosion (dilation). In fact no adder is required in erosion and dilation operation because all values of the structuring element are zero. After the opening operation, an adder is used to subtract the estimated baseline from the input signal.

3.2. Performance of the THT baseline restoration method

To demonstrate the performance of the THT method in the FPGA hardware, the SignalTap logic analyzer is used to obtain the data from the FPGA memory through the joint test action group (JTAG) hardware debugger in real time. The result of the THT method is shown in Fig. 5, where fragments of digital signals under a 300 mV sinusoidal shift of baseline (in time frames of 50 μs) from SignalTap ii in FPGA are shown. The test signal is almost consistent with the characteristic of the HPXe detectors under external acoustic noise [17]. Although the pulse amplitude and baseline of each fragment are different, the estimated baseline corresponds to the bottom of the test signal, and the baseline of each fragment comes to around zero level after using the THT method. Thus, the THT method can restrain the shift of baseline.

Fig. 6 shows the baseline restoration performance of various methods, such as Ortec 926, the THT method, the BLRT method, and the NBLR method. Their energy resolutions at 662 keV were analyzed under different shift levels of baseline. When the shift of baseline becomes close to 50 mV, the energy resolution deteriorates dramatically from 2.63% to 8.82% with the NBLR method because the pulse amplitude values are seriously affected by the baseline fluctuations. Ortec 926 is more stable than the NBLR method, but it could hardly work at 8.63% energy resolution under 200 mV shift of baseline. No specialized baseline restoration occurs in Ortec 926; an ADC control, which depends on zero-level, lower-level, and upper-level discriminators could incompletely resolve the shift of baseline. The energy resolutions with the THT method (4.49%) and the BLRT method (6.64%) are acceptable under the 900 mV shift of baseline. The BLRT method subtracts the trapezoid bottom averaging from the trapezoid top averaging, and the averaging processes can reduce noise fluctuations in test signals. Different from the BLRT method, the THT method does not involve any averaging process. Thus, noise fluctuations seriously affect energy resolution. The

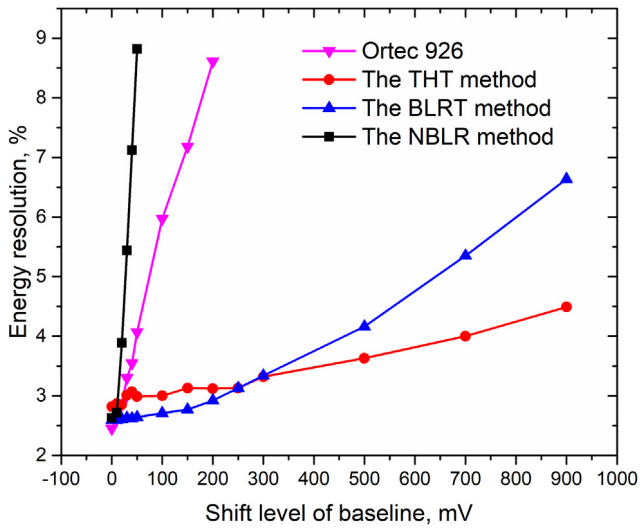

Fig. 6. Baseline restoration performance of various methods.

energy resolution with the THT method has no advantage initially. As the shift level of baseline increases, its effect on energy resolution gradually exceeds noise fluctuations. At the same time, the energy resolution with the THT method gradually exceeds that with the BLRT method. Therefore, the THT method has a better baseline restoration performance than the BLRT method.

Although the THT and BLRT methods provide positive performance in baseline restoration, energy resolutions still deteriorate slowly as the shift level of baseline increases. Fig. 7 shows the baseline restoration processes of the THT and BLRT methods under serious shift of baseline. The estimated baseline obtained by the THT method is always close to the bottom of the test signal, as shown in Fig. 7(a); thus, the THT method has the baseline recovery capability. However, the estimated baseline is evidently non-smooth with a gap below the pulse, and the pulse amplitude has a deficit for the gap, resulting in a reduction in performance. As shown in Fig. 7(b), the shift of baseline still exists after trapezoidal pulse shaping. In general, the baseline value below the pulse (ideal baseline averaging) is approximately the same as the baseline value before pulse arrival (actual baseline averaging) without the shift of baseline; thus, an accurate pulse amplitude can be obtained by the BLRT method. As the shift level of baseline increases, the difference between ideal baseline averaging and actual baseline averaging becomes evident, and the energy resolution becomes considerably poor due to inaccurate pulse amplitudes. Therefore, the increasingly significant deviation between the ideal baseline and estimated baseline negatively influences the THT and BLRT methods under serious shift of baseline.

4. IBLR baseline restoration method

4.1. Principle of the IBLR baseline restoration method

The traditional mathematical morphology uses a fixed array as structuring element; thus, the estimated baseline obtained by the THT method has similar characteristics below the pulses. However, the baseline characteristics below each pulse are different under the shift of baseline, and the traditional fixed structuring element is not suitable for the shift of baseline. In addition, no conflicts exist between mathematical morphology and the BLRT method due to the different positions and processing modes in the digital multichannel analyzer. Therefore, the IBLR method, which combines mathematical morphology and the BLRT method, was proposed in this work. In this case, the mathematical morphology could automatically adjust structuring elements according to the characteristic of the baseline in real time.

Although the baseline values are different before and after pulse arrival, their variation trends are approximately similar. A piece of variation trend before pulse arrival was extracted as the structuring element, and the erosion result is shown in Fig. 8(b). The fitting curve of the test signal baseline and that of the erosion result are almost parallel; their slopes are 0.01001 and 0.00999, respectively, and there is no gap below the pulse. Generally, the erosion result should be dilated by the structuring element to obtain the estimated baseline in the THT method. However, the dilation consumes a large amount of logic resources in FPGA. The erosion result was subtracted from the test signal directly. As shown in Fig. 8(c), the signal obtained by subtracting the erosion result from the test signal has a horizontal baseline with a DC offset. The DC offset is amplified by the trapezoidal pulse shaping [26], and it can be eliminated by the BLRT method for the stable horizontal baseline. Therefore, the deficiency caused by omitting the dilation can be resolved by the BLRT method. In addition, the BLRT method not only consumes less logical resources than dilation but also reduces noise fluctuations. Therefore, pulse amplitude can be accurately measured without the influence of shift of baseline.

4.2. Design of the IBLR baseline restoration algorithm in FPGA

The IBLR baseline restoration algorithm combines mathematical morphology and the BLRT method. No improvement in the BLRT method was observed, and the key of the IBLR method is mathematical morphology, which can automatically adjust structuring element in real

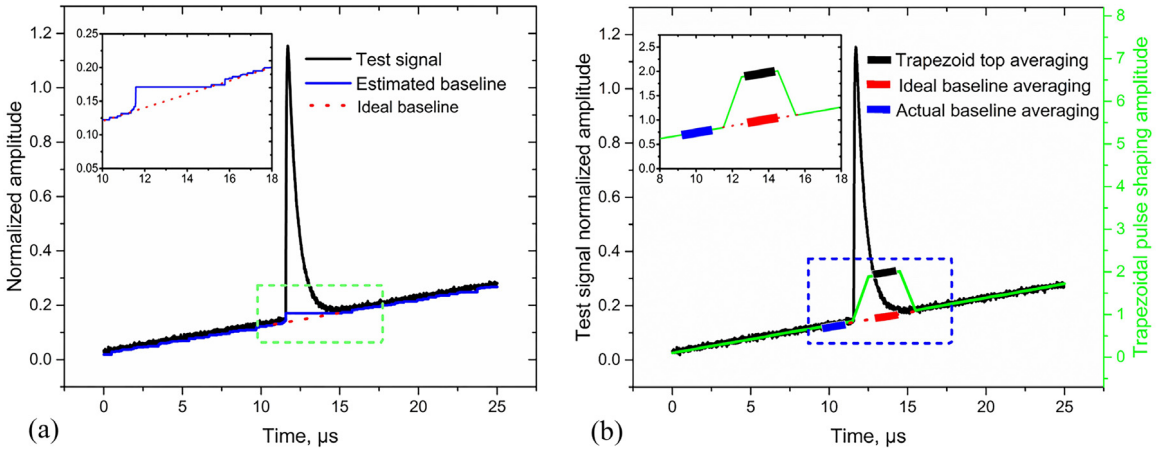

Fig. 7. Baseline restoration processes; (a) THT method, and (b) BLRT method. (For interpretation of the references to colour in this figure legend, the reader is referred to the web version of this article).

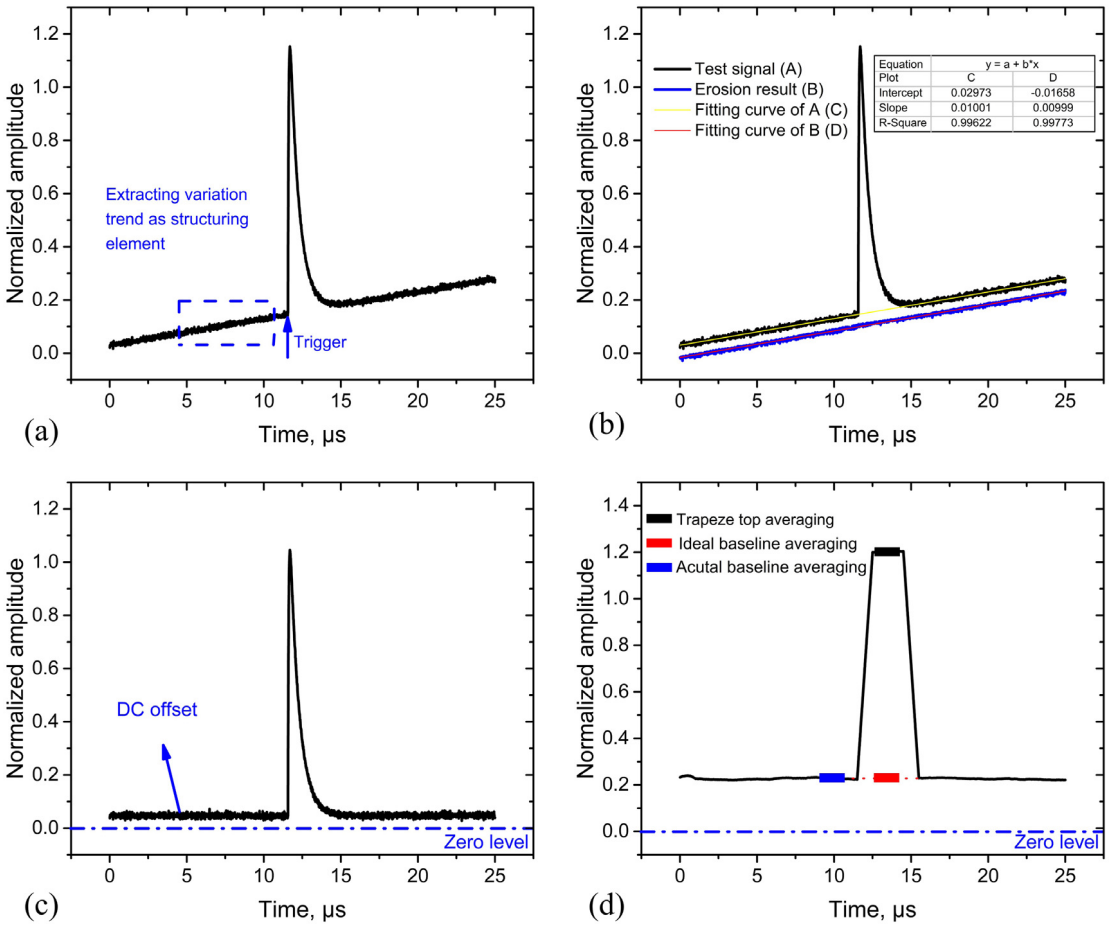

Fig. 8. Steps of the IBLR method: (a) extracting the structuring element in real time, (b) erosion, (c) subtracting the erosion result from the test signal, and (d) trapezoidal pulse shaping and the BLRT. (For interpretation of the references to colour in this figure legend, the reader is referred to the web version of this article.).

time. Fig. 9 shows the logic diagram of the mathematical morphology part in FPGA. The top level module includes pulse trigger, extracting the structuring element, and removing the erosion result. Pulse trigger is used to judge whether a pulse exists. Sufficient data for extracting the structuring element are required between the pulse and previous one. Extracting the structuring element is performed to obtain the variation trend of the baseline before pulse arrival as the structuring element. The variation trend of the baseline should be an array, where the first element is zero. In removing the erosion result module, erosion occurs with the structuring element after extraction, and then the erosion result is removed from the test signal.

4.3. Performance of the IBLR baseline restoration method

The detector with the IBLR method was tested to characterize the performance of this method, and the performance of the IBLR method is shown in Fig. 10. Fig. 10(a) shows that the energy resolution of detector with the IBLR method under the different shift levels of baseline. It maintains an excellent energy resolution (2.64%) under 900 mV shift of baseline. To prove the stability of the baseline restoration performance, we used line fitting to indicate the decline trend of the energy resolution. The result of line fitting shows that the energy resolutions are hardly reduced due to the small slope (3.05E−5). The addition of baseline restoration can influence the energy resolution under normal operation; thus, it is necessary to pay attention to the energy resolution before and after adding the baseline restoration. Fig. 10(b) shows that the energy resolution with various baseline restoration method under normal and shift of baseline operations, and the energy resolution, which is under normal operation, is 2.63% before adding baseline restoration method. After adding various baseline restoration methods, the order of energy resolution is BLRT > IBLR > THT. The energy resolution worsens after adding the THT method because the estimated baseline and test signal contain noise fluctuations. When the estimated baseline is subtracted from the test signal, the noise fluctuations are amplified. Averaging processes, which can reduce the influence of noise fluctuations, exist to improve energy resolutions in the IBLR and BLRT methods. When the HPXe detector works under serious shift of baseline (900 mV), the order of the performance for various baseline restorations is IBLR > THT > BLRT, and the energy resolutions with the IBLR method are constant before and after serious shift of baseline.

The frequency of noise is important for the detector, because the efficiency of the algorithms should depend on the frequency and noise characteristics. The resonance frequency responses of the HPXe detector is almost at low frequency [15,16,27]. Table 1 shows that the energy resolution of detector with IBLR method under various frequencies of 900 mV shift of baseline. It can be seen that the IBLR method is effective at the low frequency.

5. Results of HPXe detector with the IBLR method under high external acoustic noise

The IBLR method achieves excellent baseline restoration; it can be applied to remove the vibroacoustic effects of HPXe detectors. To study the HPXe detector's response to vibroacoustic effects with the

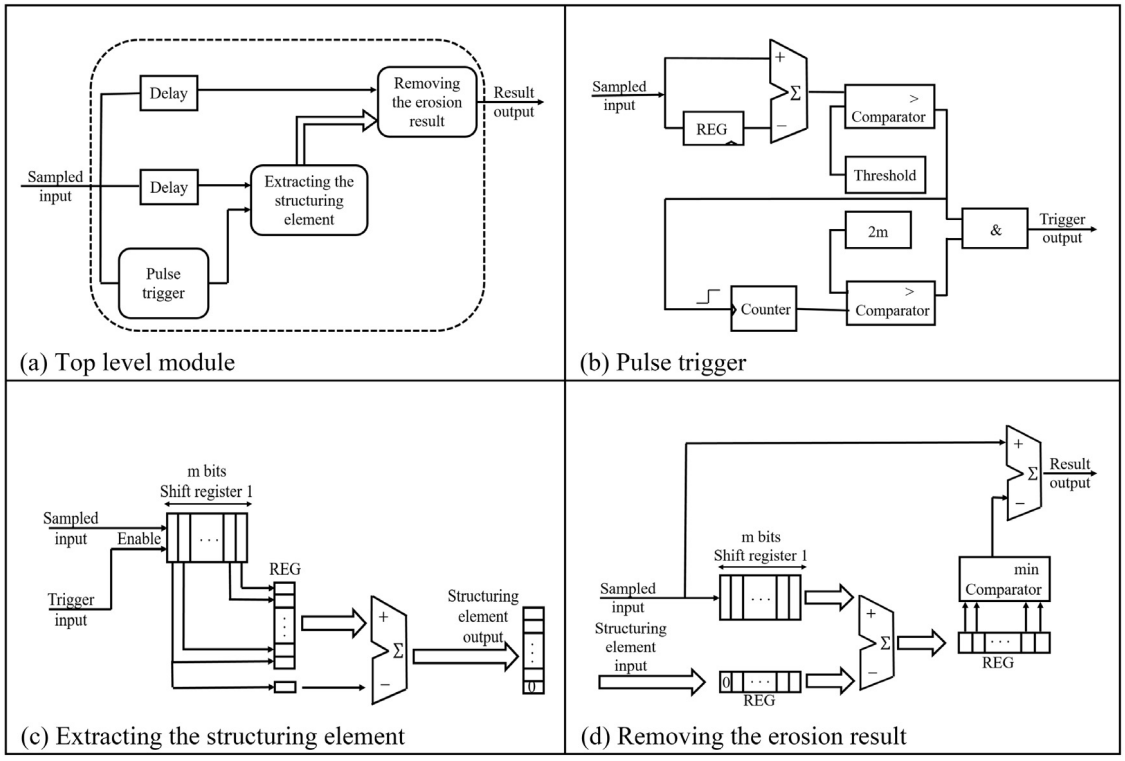

Fig. 9. Implementation of mathematical morphology part with structuring element adjusted in real time in FPGA: (a) top level module, (b) pulse trigger module, (c) extracting the structuring element module, and (d) removing the erosion result module.

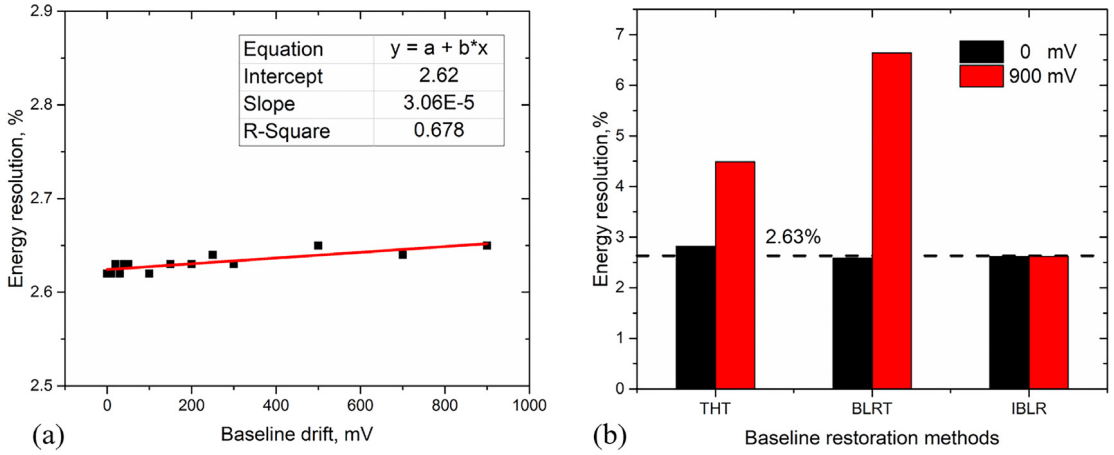

Fig. 10. Baseline restoration performance of the IBLR method. (For interpretation of the references to colour in this figure legend, the reader is referred to the web version of this article).

IBLR method, we used a speaker with sinusoidal noise. Fig. 11 shows the HPXe detector's energy spectra of Cs137 for different baseline restorations under 90 dB external acoustic noise. The energy spectrum measured without external acoustic noise was set as a standard. For the BLRT method, the gamma ray absorption peak was distorted seriously, and the pulse throughput declined evidently. For the THT method, a small reduction in energy resolution was observed. However, the energy spectrum with the IBLR method was virtually unaffected by the 90 dB external acoustic noise; it almost overlapped with the standard spectrum. Table 2 shown the energy resolution of the detector after applying different methods under different noise levels. Compared to the other two methods, the IBLR method had superior acoustic noise resistance, and maintained an outstanding energy resolution under 90 dB. Therefore, the HPXe detector with the IBLR method can normally operate under the high acoustic noise environments with a constant spectrometric characteristic.

6. Conclusion

This study presented an application of mathematical morphology as baseline restoration to remove the vibroacoustic effects of HPXe detectors. This algorithm was implemented in DMCA based on FPGA. The traditional mathematical morphology baseline restoration called the THT method was demonstrated to obtain a better baseline restoration performance than the BLRT method. The IBLR method, which combines mathematical morphology and the BLRT method, was proposed; the mathematical morphology could automatically adjust the structuring element before each pulse arrival. The experimental results showed that

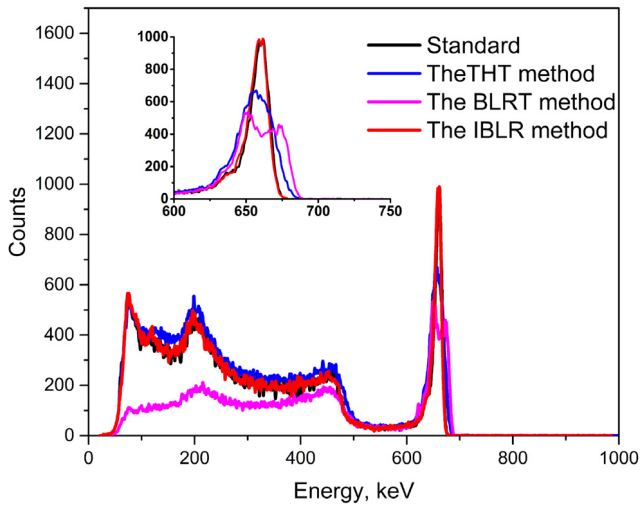

Fig. 11. Energy spectrum of various approaches under 90 dB external acoustic noise (with energy spectrum measured without external acoustic noise as a standard). (For interpretation of the references to colour in this figure legend, the reader is referred to the web version of this article.).

Table 1
The energy resolution (at 662 keV) of detector with IBLR method under various frequencies.

Frequency	100 Hz	200 Hz	300 Hz	400 Hz	500 Hz	1000 Hz
Energy resolution	2.69%	2.64%	2.78%	2.74%	2.74%	2.62%
Frequency	1500 Hz	2000 Hz	2500 Hz	3000 Hz	3500 Hz	4000 Hz
Energy resolution	2.73%	2.67%	2.83%	3.02%	3.26%	3.37%

Table 2
The energy resolution (at 662 keV) after applying different algorithms under different noise level.

	50 dB	60 dB	70 dB	80 dB	90 dB
BLRT	2.59	2.71	3.54	–	–
THT	2.82	3.00	3.13	3.42	4.49
IBLR	2.62	2.63	2.63	2.65	2.70

the HPXe detector with the IBLR method could maintain an excellent energy resolution over a wide shift range of baseline and was not affected by external acoustic noise up to 90 dB.

A serious shift of baseline occurred in the HPXe detector under high external acoustic noise. The HPXe detector with the IBLR method maintained excellent energy resolution and successfully removed the shift of baseline in real time under strong acoustic noise environments. At the same time, it improved the capability of anti-vibration, thereby expanding the scope of the application of HPXe detectors.

Traditional physical methods, such as adding different sound absorbers and improving grid hardness, are efficient under 70 dB. The Butterworth filter can remove the dominant noise frequencies, but performance of detector degrades with the filter implemented under normal operation. Digital signals processing technique designed by MEPhI make a significant improvement to 90 dB. Compared with this methods, the HPXe detector with IBLR method can also operate under 90 dB. Besides it can be implemented easily in FPGA and have a potential under the higher noise level for the automatical adjustment of structuring element according to the characteristics of the baseline.

This IBLR method is not suitable for high count rate systems. When the distance between adjacent pulses is too short to extract the structuring element, it cannot be adjusted in real time. Thus, the performance of baseline restoration declines. In future work, the baseline restoration in high count rate systems should be studied, and the length of structuring elements should be adjusted intelligently.

Acknowledgments

This work was supported by the National Natural Science Foundation of China (Grant No. 11675078), the Primary Research and Development Plan of Jiangsu Province (Grant No. BE2017729), the Fundamental Research Funds for the Central Universities (Grant No. NJ20160034), the Funding of Jiangsu Innovation Program for Graduate Education (Grant No. KYLX16_0353) and the Foundation of Graduate Innovation Center in NUAA (Grant No. kfjj20170613).

References

[1] P. Wang, X. Bin Tang, P. Gong, X. Huang, L.S. Wen, Z.Y. Han, J.P. He, Design of a portable dose rate detector based on a double Geiger–Mueller counter, Nucl. Instrum. Methods Phys. Res. A 879 (2018) 147–152.
[2] D.A. Haas, P.W. Eslinger, T.W. Bowyer, I.M. Cameron, J.C. Hayes, J.D. Lowrey, H.S. Miley, Improved performance comparisons of radioxenon systems for low level releases in nuclear explosion monitoring, J. Environ. Radioact. 178–179 (2017) 127–135.
[3] R. Coulon, J. Dumazert, T. Tith, E. Rohée, K. Boudergui, Large-volume and room-temperature gamma spectrometer for environmental radiation monitoring, Nucl. Eng. Technol. 49 (2017) 1489–1494.
[4] H.S. Kim, S.H. Park, J.H. Ha, Y.K. Kim, J.K. Kim, S.Y. Cho, Performance of a high-pressure xenon ionization chamber for environmental radiation monitoring, Radiat. Meas. 43 (2008) 659–663.
[5] A.S. Novikov, S.E. Ulin, I.V. Chernysheva, V.V. Dmitrenko, V.M. Grachev, D.V. Petrenko, A.E. Shustov, Z.M. Uteshev, K.F. Vlasik, Xenon gamma-ray detector for ecological applications, J. Appl. Remote Sens. 9 (2015) 96087.
[6] S.E. Ulin, V.V. Dmitrenko, V.M. Grachev, K.F. Vlasik, Z.M. Uteshev, A.S. Novikov, Prospects of xenon gamma-ray spectrometers for environmental monitoring, Ecol. Syst. Devices. 7 (2010) 3–10.
[7] K.F. Vlasik, V.M. Grachev, V.V. Dmitrenko, S.E. Ulin, Z.M. Uteshev, Yu.T. Yurkin, Effect of proton and neutron fluxes on the spectrometric characteristics of the high-pressure xenon gamma-ray spectrometer, Instruments Exp. Tech. 41 (1998) 309–314.
[8] A.E. Bolotnikov, V.V. Dmitrenko, L.V. Chernyshova, The high pressure xenon detector for gammaray astronomy on board of the orbital station Mir, in: Proc. Int. Conf. Liq. Radiat. Detect. Their Fundam. Prop. Appl. n.d.: pp. 462–465.
[9] S. Ulin, A. Novikov, V. Dmitrenko, K. Vlasik, K. Krivova, D. Petrenko, Z. Uteshev, A. Shustov, E. Petkovich, Xenon gamma-ray spectrometer for radioactive waste controlling complex, J. Phys.: Conf. Ser. (2016) 42023.
[10] G.P. Lasché, V.V. Dmitrenko, S.E. Ulin, S. Haan, S. Hustache, V.M. Grachev, D.V. Sokolov, Z.M. Uteshev, K.F. Vlasik, R.L. Coldwell, C.J. Cray, Detection sensitivity for special nuclear materials with an advanced high-pressure xenon detector and robust fitting analysis, IEEE Trans. Nucl. Sci. 48 (2001) 325–329.
[11] A. Bolotnikov, A. Bolozdynya, R. DeVito, J. Richards, Dual-anode high-pressure xenon cylindrical ionization chamber, IEEE Trans. Nucl. Sci. 51 (2004) 1262–1269.
[12] R. Kessick, G. Tepper, A hemispherical high-pressure xenon gamma radiation spectrometer, Nucl. Instrum. Methods Phys. Res. A 490 (2002) 243–250.
[13] J.L. Lacy, A. Athanasiades, N.N. Shehad, L. Sun, T.D. Lyons, C.S. Martin, L. Bu, Cylindrical high pressure xenon spectrometer using scintillation light pulse correction, in: IEEE Nucl. Sci. Symp. Conf. Rec., IEEE, 2004, pp. 16–20.
[14] S.E. Ulin, V.V. Dmitrenko, V.M. Grachev, A cylindrical ionization chamber with a shielding mesh filled with xenon under a pressure of 50 atm, Instruments Exp. Tech. 38 (1995) 326–330.
[15] V.V. Dmitrenko, I.V. Chernysheva, Vibrostability of high pressure xenon gamma-ray detectors, Nucl. Sci. (2000) 665–669.
[16] A. Seifert, B. Milbrath, W.K. Pitts, E. Smith, Implementation of a noise mitigation strategy for a high-pressure xenon detector, in: IEEE Nucl. Sci. Symp. Conf. Rec., IEEE, 2005, pp. 1262–1266.
[17] A.S. Novikov, S.E. Ulin, V.V. Dmitrenko, Z.M. Uteshev, K.F. Vlasik, V.M. Grachev, Y.V. Efremenko, I.V. Chernysheva, A.E. Shustov, New modification of xenon gamma-ray detector with high energy resolution, Opt. Eng. 53 (2013) 021108.
[18] Glenn F. Knoll, Radiation Detection and Measurement, John Wiley & Sons, 1999.
[19] S.E. Ulin, V.V. Dmitrenko, V.M. Grachev, O.N. Kondakova, S.V. Krivov, S.I. Sutchkov, Z.M. Uteshev, K.F. Vlasik, Yu.T. Yurkin, I.V. Chernycheva, High-pressure xenon cylindrical ionization chamber with a shielding mesh, in: Gamma-Ray Detect. Phys. Appl, International Society for Optics and Photonics, 1994, pp. 28–33.
[20] Z. Guzik, T. Krakowski, Algorithms for digital gamma-ray spectroscopy, Nukleonika 58 (2013) 333–338.
[21] Y. Sun, K.L. Chan, S.M. Krishnan, Characteristic wave detection in ECG signal using morphological transform, BMC Cardiovasc. Disord. 5 (2005) 1–7.
[22] R. Perez-Pueyo, M.J. Soneira, S. Ruiz-Moreno, Morphology-based automated baseline removal for raman spectra of artistic pigments, Appl. Spectrosc. 64 (2010) 595–600.
[23] S.A. Taouli, ECG signal denoising by morphological top-hat transform, Glob. J. Comput. Sci. Technol. 13 (2013).

[24] C.J. Gan, Y.H. Tan, Parameter optimization of structure elements in top-hat transform for the R-wave location detection in ECG, Acta Electron. Sin. 12 (2012) 943–948.
[25] Z. Li, D.J. Zhan, J.J. Wang, J. Huang, Q.S. Xu, Z.M. Zhang, Y.B. Zheng, Y.Z. Liang, H. Wang, Morphological weighted penalized least squares for background correction, Analyst 138 (2013) 4483–4492.
[26] G. Zeng, J. Yang, T. Hu, L. Ge, X. Ouyang, Q. Zhang, Y. Gu, Baseline restoration technique based on symmetrical zero-area trapezoidal pulse shaper, Nucl. Instrum. Methods Phys. Res. A 858 (2017) 57–61.
[27] A.G. Beyerle, B. Cabrera-Palmer, A.C. Little, Second generation high-pressure xenon gamma-ray detector, in: Nucl. Sci. Symp. Conf. Rec. 2007 NSS'07 IEEE, IEEE, 2007, pp. 613–615.